Recycling of continental crust into the mantle as revealed by Kytlym dunite zircons, Ural Mts, Russia

F. Bea,[1]* G. B. Fershtater,[2] P. Montero,[1] M. Whitehouse,[3] V. Ya. Levin,[2] J. H. Scarrow,[1] H. Austrheim[4] and E. V. Pushkariev[2]

[1]*Department of Mineralogy and Petrology, Campus Fuentenueva, University of Granada, 18002 Granada, Spain;* [2]*Institute of Geology and Geochemistry, Russian Academy of Sciences. Pochtovi per. 7, 620151 Ekaterinburg, Russia;* [3]*Swedish Museum of Natural History, Box 50007, SE-104 05 Stockholm, Sweden;* [4]*Mineralogisk-Geologisk Museum, Sars Gate 1, Toyen, 0562 Oslo, Norway*

ABSTRACT

The presence of zircons of crustal origin in the dunites of Kytlym, a subduction-related concentrically zoned dunite–clinopyroxenite–gabbro massif of the Urals Platinum-Bearing Belt, may provide the first direct evidence of the recycling of continental crust into the mantle. Zircons were part of subducted sediments that melted to produce silicic magmas with entrained restitic zircons. These melts induced partial melting in the overlying mantle, which later crystallized as the Kytlym massif. Zircons rapidly captured into early formed dunites were prevented from dissolving completely and underwent different degrees of recrystallization. A few crystals still record their original ages, which range from ~410 Myr to ~2800 Myr, thus revealing a different origin. The majority, however, recrystallized in the presence of a limited amount of melt and record the diapir formation, 350–370 Ma, which was coeval with the Uralian high-pressure metamorphism. Lastly, several grains record an age of ~330 Myr, which is identical, within error, to the Rb–Sr age of the tilaitic gabbros, (337 ± 22 Myr), and may, therefore, represent the crystallization age of the last melts formed during the evolution of Kytlym.

Terra Nova, 13, 407–412, 2001

Introduction

The recycling of continental crust into the mantle is a process that, until now, has been inferred only through indirect geophysical or geochemical considerations (e.g. Austrheim, 1991; LePichon *et al.*, 1992; Carlson, 1995; Stern and Kilian, 1996; Jahn *et al.*, 1999). Mineralogical evidence of this phenomenon may be gathered from the Kytlym massif, a subduction-related mafic-ultramafic complex of the Urals Platinum-Bearing Belt (UPBB), whose dunites contain sparsely distributed zircons discovered during the course of diamond prospecting. Given that this mineral has never been found before in dunites, and that it has not been found in thin section, it was important to check using a contamination-free method whether its presence in Kytlym was real. In order to do this, about 1 kg of rock was processed, first by breaking it with a hammer and then by submerging rock fragments, previously heated to ~900 °C, into deionized water. The disaggregated product was then attacked until dryness with HF, dissolving the precipitates in HCl and repeating the procedure several times so removing all major silicates. The last residuum was studied using scanning electron microscopy in order to identify zircons. Positive results were obtained in two independent trials carried out in Ekaterinburg and Granada.

*Correspondence: Dr F. Bea, Department of Mineralogy and Petrology, Campus Fuentenueva, University of Granada, 18002 Granada, Spain. Tel.: +34 958246176; fax: +34 958243368; e-mail: fbea@goliat.ugr.es

Geological background

The Urals form a N–S-trending, upper Palaeozoic mobile belt that extends for more than 2500 km between the eastern European and the western Siberian–Kazakh cratons (Zonenshain *et al.*, 1990; Matte, 1995). The Uralian cycle began in the late Cambrian to early Ordovician with rifting and development of a passive margin on the eastern European Craton (EEC) (Puchkov, 1997). Throughout the Palaeozoic, the Pre-Uralian ocean was host to arc and back-arc formation (Zonenshain *et al.*, 1984). The main collisional event in the Middle–Southern Urals orogeny – during the Late Devonian to early Carboniferous – occurred when EEC continental lithosphere was subducted beneath the Magnitogorsk (in the South) and Tagil (in the North) oceanic arcs, resulting in high-pressure metamorphism (Puchkov, 1997). In the Late Carboniferous to Permian there was a final collision between the East European Craton, outboard terranes, and the Siberian craton (Matte, 1995). The UPBB (Efimov and Efimova, 1967; Fershtater *et al.*, 1997, 1999) is located in the northern half of the Urals, west of the Tagil arc. Its backbone is a lineament of supra-subduction concentrically zoned dunite–clinopyroxenite–gabbro massifs (Alaskan type) intruded in the Palaeozoic accreted oceanic terranes (Fershtater *et al.*, 1999; Ivanov *et al.*, 1999). The largest and most complex body of the UPPB is Kytlym (59°30′N, 59°50′E) (Efimov and Efimova, 1967). It comprises dunites, composed of 96–98 wt% olivine (Fa_{8-10}) with minor diopside and chromite, clinopyroxenites and tilaite (low-Al, high-Ca melanocratic Cr-diopside gabbro), which have marked subduction-related compositional characteristics: elevated $^{87}Sr/^{86}Sr$ (360 Myr) ~0.7040, and ε_{Nd} (360 Myr) ~4–5; marked chondrite-normalized LREE to HREE enrichment, La_N/Yb_N 6.5–7.6; and, relative to MORB, moderately elevated large ion lithophile elements with high Rb/K, positive anomalies of K, Pb and Sr, and depleted Ta, Nb and Ti (Fig. 1). These features are consistent with a significant sediment–melt component input (cf. Plank and Langmuir, 1998) and make Kytlym different from other subduction-related mafic rocks of the Urals, such as those of Verkhisetsk or

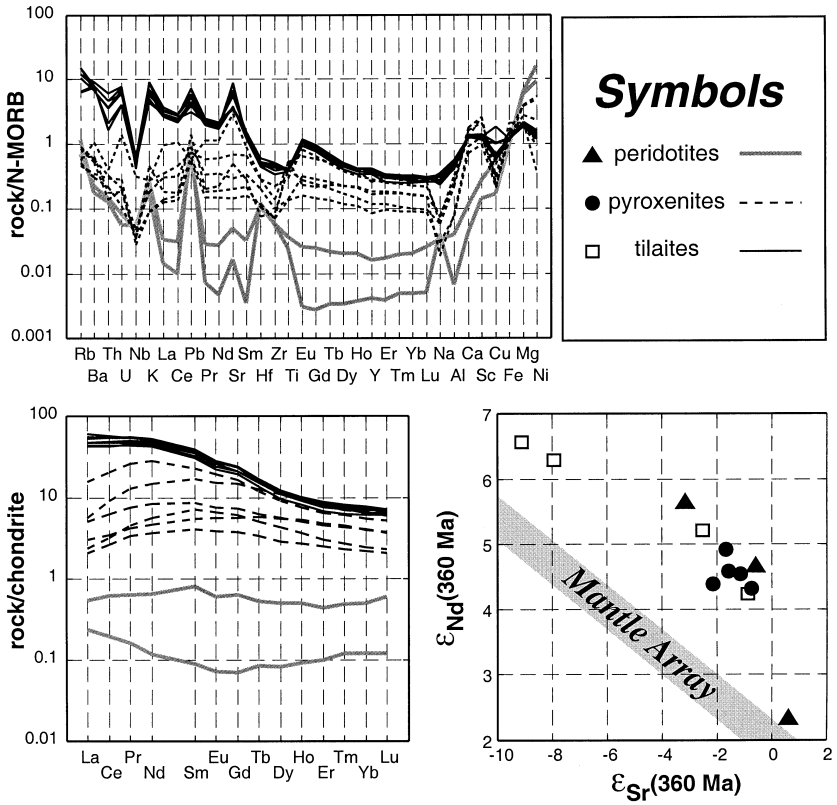

Fig. 1 N-MORB-normalized trace element, chondrite-normalized REE concentration, and ε_{Nd}(360 Myr) vs. ε_{Sr}(360 Myr) plots of Kytlym dunites, clinopyroxenites and tilaites (unpublished data of authors and Scarrow *et al.* in rev.). Note that all rocks have an arc-magma signature, with features typical of a subducted sediment input, including depleted Nb and elevated Pb, K and Sr relative to adjacent elements. Note also the elevated ε_{Sr}(360 Myr) for a given ε_{Nd}(360 Myr) with respect to the mantle array.

Syrostan, whose composition indicates a slab-derived fluid component (Scarrow *et al.* in rev.).

Methods

Twenty zircon grains were separated from 150 kg of zircon-bearing dunite slabs crushed to a grain size of < 0.25 mm, using a vibrating concentration table, then magnetic separators and finally heavy liquids. Carefully cleaned machinery never previously used for processing silicate rocks was utilized to avoid contamination with foreign zircons. Sixteen of the grains were euhedral or subhedral, colourless or yellowish, and four were rounded and purplish. Five grains of the first population and two of the second were analysed by $^{207}Pb/^{206}Pb$ single-grain stepwise-evaporation analysis (Kober, 1986, 1987) at the University of Granada (Table 1). Zircon grains were mounted on canoe-shaped Re evaporation filaments and heated until the lead beam reached an intensity of ~200–400 ^{206}Pb ions per second. Lead was collected on the ionization filament for 20–30 min, and was afterwards analysed in five blocks with seven scans per block. Once the analysis was finished, a new evaporation step was started by heating the zircon on the evaporation filament to a higher temperature than in the previous step (usually increasing the current by 50–100 mA) and analysing on the ionization filament as before. The procedure was repeated until all the lead was exhausted from the zircon. The number of steps depended on the size and lead content of each zircon. Data acquisition was performed in dynamic mode (peak hopping), using a secondary electron multiplier (SEM) as detector with the 206–204–206–207–208 mass sequence. The mass-ratio 204/206 was monitored to detect and, if necessary, correct for common lead. Factors for common lead correction were calculated by iteration from the $^{204}Pb/^{206}Pb$ and $^{204}Pb/^{207}Pb$ ratios provided by the Stacey and Kramers (1975) model at the calculated age, until convergence to a constant value. Mass fractionation was corrected by multiplying by $\sqrt{(207/206)}$. Standard Errors for each step were calculated according to the formula: $SE = 2\sigma/\sqrt{n}$. However, the 2σ confidence interval for the final age is given by the interval $X \pm t(0.025)\sigma/\sqrt{n}$, where X and σ are the average and the SD of measured steps, n is the number of steps, and $t(0.025)$ is the upper (0.025) point of the t distribution for n–1 degrees of freedom (see Johnson and Bhattacharyya, 1984, p.296).

The remaining 13 grains were studied by cathodoluminiscence imaging and analysed for U–Th–Pb using a Cameca IMS1270 ion microprobe at the Nordsim facility in Stockholm. Analytical methods broadly follow those described by Whitehouse *et al.* (1999 and references therein). U/Pb and Th/Pb ratios were calibrated using as standard the CRPG 91500 reference zircon (1065 Myr age; Wiedenbeck *et al.*, 1995) and includes a propagated error component from replicate analyses of the standard. Errors on $^{207}Pb/^{206}Pb$ ratios are either the observed analytical uncertainty or the counting statistics error, whichever is highest. Common Pb corrections assume that most contaminant Pb is present on the surface of the analysed grains, introduced from the sample preparation process (e.g. Zeck and Whitehouse, 1999), and has a composition that can be approximated using the Stacey and Kramers (1975) model for the present day. For grains with ages < 500 Myr, Table 2 presents the '207-corrected' ages which are calculated by projecting the uncorrected analysis onto concordia from the assumed common $^{207}Pb/^{206}Pb$ composition. In most cases, however, the amount of common Pb, revealed by monitoring ^{204}Pb, is relatively small and has little influence on the interpreted age. All ages are calculated using the decay constant recommendations of Steiger and Jäger (1977).

Table 1 Pb/Pb stepwise evaporation results of seven zircons grains, 1–5 were euhedral or subhedral, colourless or yellowish, whereas 6 and 7 were rounded and purplish. $^{207}Pb/^{206}Pb$-corrected values were obtained correcting the analytical values of $^{207}Pb/^{206}Pb$ for common lead ($^{204}Pb/^{206}Pb$) using Stacey and Kramers' (1975) model. Age errors are at the 2σ level

Grain no.	Step	$^{204}Pb/^{206}Pb$	$^{207}Pb/^{206}Pb$	% error (2σ)	$^{207}Pb/^{206}Pb$ (corr.)	Age (Myr)
1	1	0.000216	0.056126	0.42	0.053093	333 ± 9
2	1	0.000068	0.053895	0.33	0.053028	330 ± 7
2	2	0.000388	0.058666	0.38	0.05311	334 ± 9
2	3	0.000409	0.059003	0.52	0.053146	335 ± 12
3	1	0.000110	0.055113	0.47	0.053624	355 ± 10
3	2	0.000308	0.058014	0.28	0.053635	356 ± 6
3	3	0.000097	0.055112	0.57	0.053823	364 ± 12
4	1	0.000040	0.054095	0.28	0.053629	357 ± 7
4	2	0.000208	0.056860	0.28	0.053942	369 ± 7
5	1	0.000089	0.054742	0.60	0.053560	355 ± 15
5	2	0.000086	0.054835	0.50	0.053696	358 ± 11
5	3	0.000091	0.054993	0.47	0.053793	362 ± 10
5	4	0.000103	0.055333	0.60	0.053954	369 ± 13
5	5	0.000132	0.056044	1.00	0.542440	381 ± 22
6	1	0.000549	0.088203	1.20	0.080637	1213 ± 23
6	2	0.000195	0.085613	0.92	0.083055	1270 ± 18
7	1	0.000134	0.132261	1.50	0.130811	2109 ± 23
7	2	0.000010	0.170203	0.16	0.169816	2556 ± 2
7	3	0.000033	0.189035	1.00	0.189093	2734 ± 16
7	4	0.000008	0.198257	1.40	0.198632	2815 ± 23
7	5	0.000008	0.199743	0.39	0.200122	2827 ± 6
7	6	0.000035	0.201355	0.60	0.201424	2838 ± 10

Table 2 Ion microprobe chemical composition and isotope ratios of Kytlym zircons

Number											
Grain	Analysis	Group	U (ppm)	Pb (ppm)	Th/U*	f_{206}† (%)	$^{207}Pb/^{206}Pb$	% error	$^{206}Pb/^{238}U$	% error	Age (Myr)‡
1	1	IV	239	17	0.40	4.83	0.09418	3.45	0.05300	4.28	315 ± 13
1	2	IV	54	3	0.20	0.51	0.05542	2.18	0.05063	4.28	317 ± 13
1	3	IV	150	9	0.47	0.07	0.05233	1.36	0.05201	4.28	327 ± 13
2	1	IV	140	8	0.30	0.37	0.05321	1.38	0.05253	4.32	329 ± 14
3	1	III	373	26	0.92	0.25	0.05448	0.81	0.05419	4.28	339 ± 14
4	1	III	54	4	0.44	0.39	0.05226	2.44	0.05611	4.30	352 ± 14
4	2	III	106	7	0.60	0.13	0.05531	1.48	0.05636	4.28	352 ± 14
5	1	III	107	8	0.63	0.19	0.05323	1.83	0.05756	4.27	360 ± 15
5	2	III	109	8	0.54	0.24	0.05411	1.44	0.05769	4.28	361 ± 15
6	1	III	277	18	0.25	0.12	0.05429	0.96	0.05839	4.28	365 ± 15
6	2	III	89	6	0.61	0.25	0.05363	1.55	0.05838	4.27	365 ± 15
7	1	III	71	5	0.78	0.17	0.05502	2.09	0.05882	4.29	367 ± 15
7	2	III	99	7	0.72	0.20	0.05369	1.53	0.05897	4.29	369 ± 15
8	1	III	52	4	0.44	0.32	0.05337	2.12	0.05986	4.28	375 ± 15
9	1	III	104	8	1.01	0.34	0.05379	1.47	0.06093	4.28	381 ± 16
10	1	II	123	9	0.28	0.50	0.05854	1.49	0.06446	4.27	400 ± 16
11	1	II	63	5	0.40	0.17	0.05710	1.80	0.06949	4.27	432 ± 18
11	2	II	57	5	0.37	0.15	0.05622	2.32	0.06993	4.29	435 ± 18
12	1	I	331	166	1.31	0.02	0.11020	0.29	0.34975	4.27	1802 ± 5
13	1	I	143	75	1.56	0.03	0.11020	0.41	0.35066	4.27	1802 ± 7

*Th/U ratios are measured directly using ThO and U signals and referenced to the standard zircon 91500. †f_{206} is the amount (in percentage) of ^{206}Pb contributed by common Pb; estimated from measured ^{204}Pb. ‡Ages below 500 Myr are 207-corrected; ages for the two group I samples are uncorrected $^{207}Pb/^{206}Pb$ ages.

Results

Both stepwise evaporation and ion microprobe methods produced the same age pattern (Fig. 2), which, together with morphology and cathodoluminiscence images, seems to indicate the existence of four populations of probable crustal origin. The oldest population (I) comprises four rounded purplish grains showing no evidence of metamorphic recrystallization. They recorded ages from ~1200 to ~2841 ± 10 Myr and are rich in Th and U (Table 2) with marked oscillatory zoning and eccentric external boundaries with respect to their internal morphology (Fig. 3A).

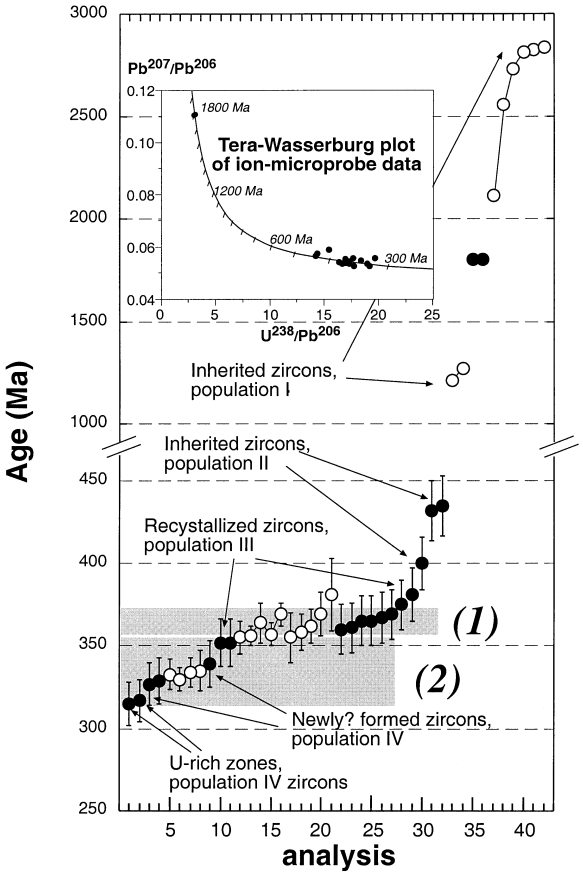

Fig. 2 Single zircon $^{207}Pb/^{206}Pb$ stepwise evaporation (open circles) and U–Pb ion microprobe (black dots) ages of Kytlym dunite zircons. Where symbols are joined, this implies analyses on the same crystal (SIMS) or plating steps from the same crystal (evaporation). Grey bands (1) and (2) represent the Rb–Sr age of the high-pressure metamorphism in the Urals and the tilaites, respectively. See text.

Population II consists of two grains, one rounded purplish (Fig. 3B) and the other more angular, which under cathodoluminiscence show similar features to population I but have low Th and U, and yielded ages from 410 to 430 Myr. Population III comprises 9 grains with ages from 370 to 352 Myr, equivalent to the age range determined for Uralian high-pressure metamorphism (Glodny *et al.*, 1999). These grains are subhedral, with frequent corrosion structures and marked patchy zoning (Fig. 3C,D). Population IV comprises five grains that are mostly euhedral and oscillatory zoned (Fig. 3E), with ages of 327–340 Myr, which is the age of associated tilaitic gabbros, dated by Rb–Sr at 337 ± 22 Myr (2σ, unpubl. data). One grain (Fig. 3F) also shows younger U–rich zones that yielded a concordant U–Pb age of 317 ± 13 Myr (1σ).

Discussion

Given the refractory character of zircon, and as this mineral has never been found before in dunites, is it possible that its occurrence in Kytlym is due to the survival of recycled crustal material in the mantle. According to available geochemical and isotopic evidence, Kytlym is a subduction-related body generated in the mantle wedge by partial melting triggered by subducted sediment-derived silicic melts. Therefore, the zircons' history can be traced as follows.

Silicic melts containing entrained restitic zircons were generated in the slab from subducted sediments and migrated upwards, triggering partial melting of mantle-wedge peridotites. These hybrid melts migrated by focused porous flow through dissolution channels, producing the replacive dunite of the core of the uprising body (Kelemen, 1990; Kelemen *et al.*, 1995). Because the solubility of zircon in melt increases with increasing temperature and decreasing silica content (Watson and Harrison, 1983), the fate of zircons entrained in initial silicic melts is to be quickly and completely dissolved once such melts are released to the mantle wedge, unless kinetic effects delay the process. During focused porous flow, the main factor controlling zircon solution kinetics is the volume of melt of zircon-containing pores; when the pore volume is small, the increasing concentration of Zr in the melt would slow down the dissolution of zircon preventing further dissolution once saturation is reached.

An investigation into the solution kinetics of a zircon grain in small melt reservoirs was carried out using the 3D dissolution equation for spherical zircon crystals of Watson (1996) and the Watson and Harrison (1983) solubility model of zircon, according to which it depends only on the SiO_2 contents and the temperature of the melt. The present authors' calculations (Fig. 4) reveal that in basaltic melts at hydrated-peridotite solidus temperature, zircon spheres with a radius of 150 μm would dissolve completely in $< 10^6$ yr if the melt reservoir diameter is > 2 mm; however, in reservoirs with a diameter of < 1 mm, zircon dissolution is slowed down as the Zr concentration approaches saturation and completely arrested before total dissolution. The limiting case would be when the melt volume is zero, i.e. when the zircon grain is directly included in a crystallizing mineral. It also follows that in those pores containing undissolved zircons and Zr-saturated melt, small fluctuations of temperature, volume, melt bulk composition, etc. can produce a complex sequence of zircon dissolution and recrystallization, with the subsequent resetting of the U–Pb isotopic system. Certainly, these calculations are a rough estimate because (i) the solubility model of Watson and Harrison (1983) was extrapolated to a melt composition and temperature for which it was not intended, and (ii) the geometry of zircon grains may not be spherical. The model, however, does not depart dramatically from the real situation, because the temperature used is only 30 °C higher than

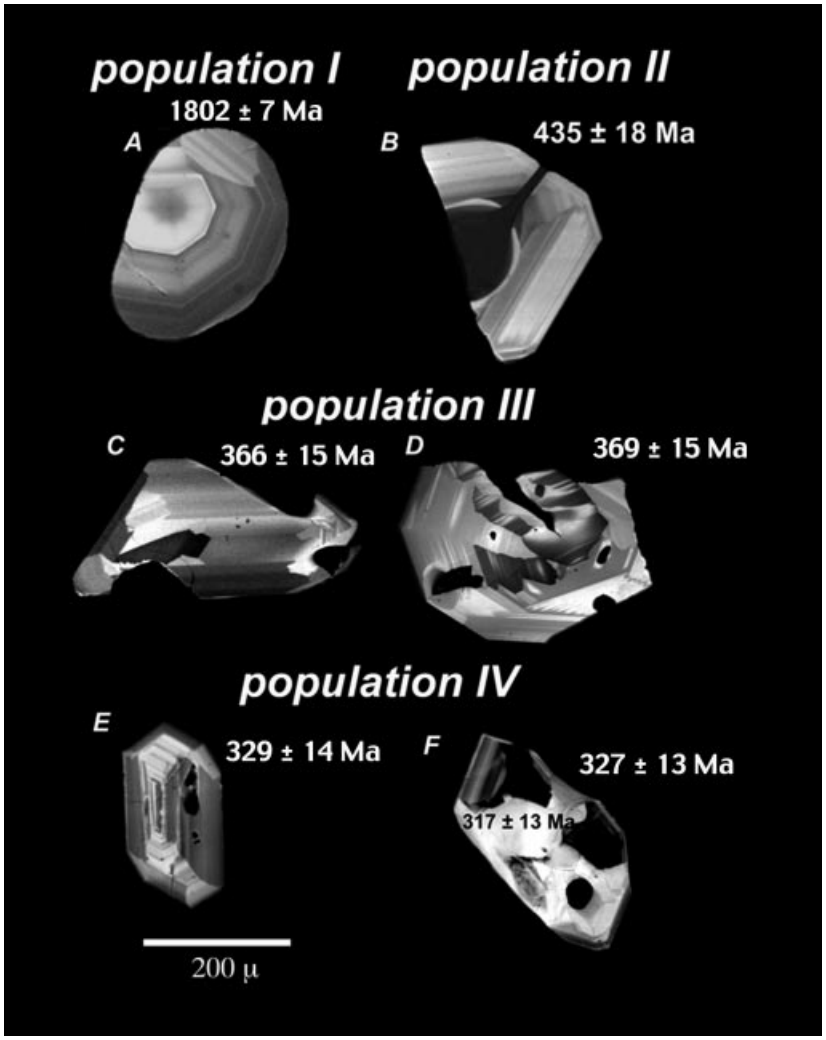

Fig. 3 Cathodolumiscence images of representative Kytlym dunite zircons: (A) and (B), inherited crustal zircons; (C) and (D), recrystallized in the presence of a limited amount of fluid; (E) and (F), grown in the presence of melt.

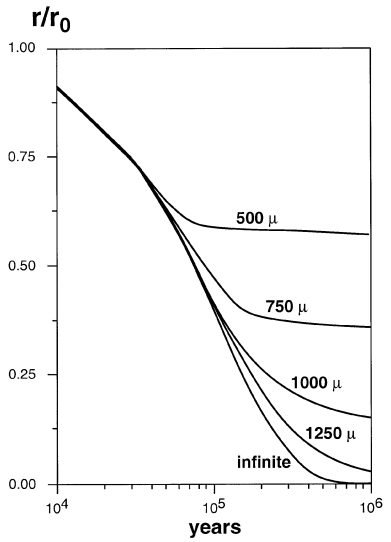

Fig. 4 Dissolution of zircon spheres (radius = 150 μm) in spherical reservoirs of basaltic melt at constant T (1050 °C) as a function of the radius of the reservoir, calculated with the 3D dissolution equation of Watson (1996). Each curve indicates the ratio between the current and initial radius of the zircon grain as a function of time for a reservoir with a given size, the radius of which is expressed in μm. Curves become nearly horizontal when the concentration of Zr in the melt approaches saturation. Note how the zircon grain dissolves totally in less than 1 Myr when the radius of the melt reservoir is larger than 1500 μm (infinite), but the dissolution is arrested after 0.1 Myr in reservoirs with a radius of 500 μm.

the 1020 °C upper limit of Watson and Harrison's (1983) experiments, and the morphology of the inherited detrital zircons tend to be spherical.

Accordingly, the following origin is suggested for the Kytlym dunite zircons. Populations I and II may represent inherited zircons rapidly included in crystallizing olivine, thus having little or no opportunity to react with the melt. They therefore still preserve their original microtexture, composition and age. The difference between the two populations suggests that they were derived from sediments with different source areas: the Palaeoproterozoic to Neoarchean materials of the Russian platform in the case of population I, and Silurian magmatic materials of the Tagil arc in the case of the population II. Population III is composed of zircons that have reacted with melt but were probably not completely dissolved because of the small volume of the pores that contained them. Their age would mark the moment at which they were included in a crystallizing phase – so preventing further reaction with the melt – and would probably indicate the beginning of partial melting in the mantle wedge. This idea finds additional support from the fact that both U–Pb and Pb–Pb age determinations cluster around 360 Myr, the age of the high-P metamorphism (Glodny *et al.*, 1999). Population IV is more difficult to interpret: its morphology and cathodoluminiscence features suggest that the grains crystallized fully from a melt. However, since their ages are close to the Rb–Sr age of the tilaites (~340 Myr), which represent the last and the most voluminous magmatic event in the buoyant Kytlym diapir (Efimov and Efimova, 1967), it is suggested tentatively that they were formed by total dissolution of zircons of populations I to III into the last melt batches percolating the core of Kytlym diapir; if these batches are sufficiently small they would have been saturated in Zr as the temperature decreased, so precipitating population IV crystals.

Conclusions

Inherited zircons have been found in a replacive dunite from the core of the concentrically zoned dunite–clinopyroxenite–gabbro subduction-related

complex of Kytlym, in the UPPB. These zircons belong to four populations. The characteristics of population I indicate that they are crustal (age, high U and Th), crystallized from a melt (euhedral oscillatory zoned) and were probably incorporated into sediments as detrital particles (their rounded external morphology is eccentric with the zoning). They most likely derived from materials of the Russian Platform. Population II had a similar origin but a younger protolith such as the Tagil-arc Silurian granitoids. Lack of recrystallization in zircon populations I and II indicates inclusion in early formed olivine crystals and therefore they preserve their protolith ages. Population III shows evidence of solid-state recrystallization (patchy zoning) in the presence of limited fluid (corroded boundaries) resulting from retention in short-lived, small-volume melt reservoirs. So, recrystallization produced a uniform age that matches Uralian high-pressure metamorphism and reflects the initial stage of the diapir formation in the mantle wedge induced by slab-derived melts. Population IV grew in the presence of melt (oscillatory zoning), and its age most probably reflects crystallization of the last magma pulses that occurred during final emplacement of the Kytlym diapir.

Acknowledgments

We are grateful to Urs Schaltegger and Piera Spadea for their thoroughly revisions of the manuscript, which greatly contributed to its improvement. We are also grateful to Jan Kramers for his assistance as associate editor. The support of Torbjörn Sunde during SIMS analyses and Chris Laurin for her help with the English is gratefully acknowledged. This is Nordsim laboratory publication 53. The Nordsim facility is supported by the Natural Science funding agencies of Denmark, Finland, Norway and Sweden. This work has been supported by the Spanish DGICYT grant PB98–1345, the EU TMR URO, and the Russian Fond for Basic Research (RFFI) grant 01–05–65184.

References

Austrheim, H., 1991. Eclogite formation and dynamics of crustal roots under continental collision areas. *Terra Nova*, **3**, 492–499.

Carlson, R.W., 1995. Isotopic inferences on the chemical structure of the mantle. *J. Geodynamics*, **20**, 365–386.

Efimov, A.A. and Efimova, L.P., 1967. *The Kytlym Platiniferous Massif*. Nedra, Moscow (in Russian).

Fershtater, G.B., Montero, P., Borodina, N.S., Pushkarev, E.V., Smirnov, V.N. and Bea, F., 1997. Uralian magmatism: an overview. *Tectonophysics*, **273**, 87–102.

Fershtater, G.B., Bea, F., Pushkarev, E.V., Garuti, G., Montero, P. and Zaccarini, F., 1999. Insight into the petrogenesis of the Ural Platinum belt: New geochemical evidence. *Geokhimiya*, **4**, 352–370 (in Russian).

Glodny, J., Austrheim, H., Bingen, B., Rusin, A. and Scarrow, J.H., 1999. New age data for HP rocks and ophiolites along the Main Uralian Fault, Russia: implications for the Uralian Orogeny. *Terra nostra*, **99**, 89–90.

Ivanov, K.S., Anikina, E.V., Efimov, A.A., Pushkarev, E.V., Fershtater, G.B. and Shmelev, V.R., 1999. *Platiniferous Belt of the Urals*. Institute of Geology and Geochemistry, Ekaterinburg (in Russian).

Jahn, B.M., Wu, F.Y., Lo, C.H. and Tsai, C.H., 1999. Crust–mantle interaction induced by deep subduction of the continental crust: Geochemical and Sr-Nd isotopic evidence from post-collisional mafic-ultramafic intrusions of the northern Dabie complex, central China. *Chem. Geol.*, **157**, 119–146.

Johnson, R. and Bhattacharyya, G., 1984. *Statistics: Principles and Methods*. Wiley, New York.

Kelemen, P.B., 1990. Reaction between ultramafic wall-rock and fractionating basaltic magma. I, Phase relations, the origin of calc-alkaline magma series, and the formation of discordant dunite. *J. Petrol.*, **31**, 51–98.

Kelemen, P.B., Whitehead, J.A., Aharonov, E. and Jordahl, K.A., 1995. Experiments on flow focusing in soluble porous media, with applications to melt extraction from the mantle. *J. Geophys. Res.-Solid Earth*, **100**, 475–496.

Kober, B., 1986. Whole-grain evaporation for $^{207}Pb/^{206}Pb$-age investigations on single zircons using a double filament thermal ionization source. *Contr. Miner. Petrol.*, **93**, 482–490.

Kober, B., 1987. Single-zircon evaporation combined with Pb^{+} emitter-bedding for $^{207}Pb/^{206}Pb$ age investigations using thermal ion mass spectrometry and implications to zirconology. *Contr. Miner. Petrol.*, **96**, 63–71.

LePichon, X., Fournier, M. and Jolivet, L., 1992. Kinematics, topography, shortening and extrusion in the India-Eurasia collision. *Tectonics*, **11**, 1085–1098.

Matte, P., 1995. Southern Urals and Variscides: comparison of their anatomies and evolutions. *Geol. Mijnb.*, **74**, 151–166.

Plank, T. and Langmuir, C.H., 1998. The chemical composition of subducting sediment and its consequences for the crust and mantle. *Chem. Geol.*, **145**, 325–394.

Puchkov, V.N., 1997. Structure and geodynamics of the Uralian orogen. In: *Orogeny Through Time* (J.-P. Burg and M. Ford, eds). *Spec. Publ. Geol. Soc. London*, **121**, 210–236.

Stacey, J.S. and Kramers, J.D., 1975. Approximation of Terrestrial lead isotope evolution by a two-stage model. *Earth Planet. Sci. Letts*, **26**, 207–221.

Steiger, R.H. and Jäger, E., 1977. Subcommision on Geochronology. Convention on the use of decay constants in geo- and cosmochronology. *Earth Planet. Sci. Letts*, **36**, 359–362.

Stern, C.R. and Kilian, R., 1996. Role of the subducted slab, mantle wedge and continental crust in the generation of adakites from the Andean Austral volcanic zone. *Contr. Miner. Petrol.*, **123**, 263–281.

Watson, E.B. and Harrison, T.M., 1983. Zircon saturation revisited: temperature and composition effects in a variety of crustal magma types. *Earth Planet. Sci. Letts*, **64**, 295–304.

Watson, E.B., 1996. Dissolution, growth and survival of zircons during crustal fusion. Kinetic principles, geological models implications for isotopic inheritance. *Trans. R. Soc. Edinb. (Earth Sci.)*, **87**, 43–56.

Whitehouse, M.J., Kamber, B. and Moorbath, S., 1999. Age significance of U-Th-Pb zircon data from early Archaean rocks of west Greenland a reassessment based on combined ion-microprobe and imaging studies. *Chem. Geol.*, **160**, 201–224.

Wiedenbeck, M., Allé, P., Corfu, F. *et al.*, 1995. Three natural zircon standards for U-Th-Pb Lu-Hf trace element and REE analysis. *Geostandards Newsl.*, **19**, 1–23.

Zeck, H.P. and Whitehouse, M.J., 1999. Hercynian, Pan-African, Proterozoic and Archean ion-microprobe zircon ages for a Betic-Rif core complex, Alpine belt, W. Mediterranean – consequences for its P-T-t path. *Contr. Miner. Petrol.*, **134**, 134–149.

Zonenshain, L.P., Korinevskiy, V.G., Kazmin, V.G., Matveenkov, V.V. and Khain, Y.V., 1984. Plate tectonic model of the South Urals. *Tectonophysics*, **109**, 95–135.

Zonenshain, L.P., Kuzmin, M.I. and Natapov, L.M., 1990. Geology of the USSR: A Plate-Tectonics Synthesis. In: *Geology of the USSR: a Plate-Tectonics Synthesis* (B.M. Page, ed.), Geodynamic Series 21, pp. 27–54. American Geophysical Union, Washington, DC.

Received 22 May 2001; revised version accepted 2 August 2001

